

This item is the archived peer-reviewed author-version of:

A combined experimental and computational approach to understanding CdS pigment oxidation in a renowned early 20th century painting

Reference:

Mayda Bacaksiz Selma, Monico Letizia, Krishnan Dileep, De Meyer Steven, Cotte Marine, Garrevoet Jan, Falkenberg Gerald, Sandu Irina C. A., Partoens Bart, Lamoen Dirk, ... - A combined experimental and computational approach to understanding CdS pigment oxidation in a renowned early 20th century painting
Chemistry of materials / American Chemical Society - ISSN 1520-5002 - 35:24(2023), p. 10403-10415
Full text (Publisher's DOI): <https://doi.org/10.1021/ACS.CHEMMATER.3C01470>
To cite this reference: <https://hdl.handle.net/10067/2028360151162165141>

A Combined Experimental and Computational Approach to Understanding CdS Pigment Oxidation in a Renowned Early 20th Century Painting

Selma Mayda^{*[a]}, *Letizia Monico*^{[b],[c],[d]}, *Dileep Krishnan*^[a], *Steven De Meyer*^[d], *Marine Cotte*^{[e],[f]}, *Jan Garrevoet*^[g], *Gerald Falkenberg*^[g], *Irina CA Sandu*^[h], *Bart Partoens*^[i], *Dirk Lamoen*^[a], *Aldo Romani*^{[b],[c]}, *Costanza Miliani*^[j], *Johan Verbeeck*^[a] and *Koen Janssens*^[d]

[a] Electron Microscopy for Materials Science (EMAT) and NANOLab Center of Excellence, Department of Physics, University of Antwerp, Groenenborgerlaan 171, 2020 Antwerp, Belgium. [b] CNR-SCITEC, Via Elce di Sotto 8, 06123 Perugia, Italy. [c] SMAArt Center of Excellence and Department of Chemistry, Biology, and Biotechnology, University of Perugia via Elce di Sotto 8, 06123 Perugia, Italy. [d] Antwerp X-ray Imaging and Spectroscopy Laboratory (AXIS) and NANOLab Center of Excellence, Department of Physics, University of Antwerp, Groenenborgerlaan 171, 2020 Antwerp, Belgium. [e] The European Synchrotron Radiation Facility (ESRF), 38000, Grenoble, France. [f] Laboratoire d'Archéologie Moléculaire et Structurale (LAMS), Sorbonne Université, CNRS, UMR8220, 4 place Jussieu, 75005 Paris, France. [g] Deutsches Elektronen-Synchrotron (DESY) Notkestr. 85, 22607 Hamburg, Germany. [h] MUNCH Museum, Section on Conservation, Edvard Munch plass 1, 0194 Oslo, Norway. [i] Condensed Matter Theory (CMT) and NANOLab Center of Excellence, Department of Physics, University of Antwerp, Groenenborgerlaan 171, 2020 Antwerp, Belgium. [j] CNR-ISPC via Cardinale Guglielmo Sanfelice 8, 80134, Naples, Italy.

ABSTRACT: Cadmium sulfide (CdS)-based yellow pigments have been used in a number of early 20th century artworks, including the *Scream* series painted by Edvard Munch. Some of such unique paintings

are threatened by the discoloration of CdS-based yellow oil paints because of the oxidation of original sulfides to sulfates. The experimental data prove that moisture and cadmium chlorides play a key role in promoting such oxidation. To clarify how these two factors effectively prompt the process, we studied the band alignment between CdS, CdCl₂, Cd(OH)Cl and the ·OH and H₃O· radicals by density functional theory (DFT) methods. Our results show that a stack of several layers of Cd(OH)Cl creates a pocket of positive holes at the Cl-terminated surface and a pocket of electrons at the OH-terminated surface, by leading in a difference in ionization energy at both surfaces. The resulting band alignment indicates that Cd(OH)Cl can indeed play the role of an oxidative catalyst for CdS in a moist environment, thus providing an explanation to experimental evidence.

1. Introduction

Cadmium sulfide-based yellows (CdS/Cd_{1-x}Zn_xS), present in a number of artworks by well-known artists, including Henri Matisse^{[1] [2] [3] [4]}, Vincent van Gogh^[5], James Ensor^[6], Pablo Picasso^[7] and Edvard Munch^[8] have been documented to suffer from discoloration, flaking, and chalking of paint films. In these cases, whitish compounds, such as cadmium sulfates (CdSO₄/CdSO₄·nH₂O)^[1-6], cadmium oxalate (CdC₂O₄)^[2-5], and cadmium carbonate (CdCO₃)^[1-4], were identified and tentatively proposed as either (photo)degradation products of the original cadmium yellow paint or as residues of the synthesis process of CdS. CdS exists with two different crystalline structures: either as hexagonal CdS (hex-CdS, with a wurzite-type structure, present in nature as the mineral greenockite) or as cubic CdS (cub-CdS, with a zinc blende-type structure, present in nature as the mineral hawleyite).

Assessment of the condition of cadmium yellow paints is complicated by the fact that the chemical stability of CdS may depend on its manufacturing process. Two routes, a “dry” method and a “wet” method, were used for synthesizing late 19th to early 20th century cadmium yellow pigments ^[9]. In the dry process, either metallic cadmium, cadmium oxide, or cadmium carbonate is calcined (ca. 300°C to 600°C) with pure sulfur in excess in an anoxic environment. The process, besides residues of starting

reagents (e.g., CdO and CdCO₃), may lead to the formation of CdSO₄ as by product, when anoxic conditions are not maintained. The wet process involves instead the precipitation of one or more cadmium salts (e.g., CdCl₂, CdSO₄, CdNO₃, and CdCO₃) with a soluble sulfide compound (e.g., Na₂S, H₂S, Na₂S₂O₃, and BaS). Cub-CdS is usually obtained from hot or acidic sulfate solutions, while the production of hex-CdS is usually favoured from chloride solutions. Small amounts of the cubic form sometimes occur in essentially hexagonal precipitates along with traces of starting reagents, depending upon variations in the conditions of precipitation. The environment of reaction influences also the degree of crystallinity and the sizes of the grain and aggregates of the precipitate ^[9-12] .

During our recent investigation of *The Scream (ca. 1910)* by Edvard Munch (MUNCH Museum, Oslo), important clues about the degradation mechanism of CdS-based paints could be obtained, having meaningful implications for the preventive conservation of this type of artworks. In *The Scream (ca. 1910)*, two different types of the cadmium yellow pigment were identified: hex-CdS and cub-CdS, with degradation phenomena mainly associated with the former subtype. Evidence was found that the hex-CdS in *The Scream (ca. 1910)* has a low degree of crystallinity and contains significant amounts of CdCO₃ along with a variable content of chlorine compounds, consistent with a synthesis *via* the wet process without calcination. Its degradation manifests itself either in the form of flaking detachment of impasto paint or as discoloration of the yellow pigment to an off-white color. On the other hand, mixtures of hex-CdS, cub-CdS and red HgS, as present in the orange paints of *The Scream (ca. 1910)*, did not show evident signs of degradation.

The nature of the alteration of the flaking impasto paint in *The Scream (ca. 1910)* as well as that of hex-CdS paint in other artworks was revealed to be an oxidation process: various amounts of CdSO₄, other sulfates, as well as sulfite species have been encountered in several investigations ^[1,5,6,7], which can be interpreted as oxidation products. In addition, both in *The Scream (ca. 1910)* and in CdS paint from early 20th C. paint tubes, different chloride-based compounds such as Cd(OH)Cl, NaCl and KCl were encountered too.

Originally the conversion of hex-CdS to cadmium sulfates in oil paints was exclusively attributed to photo-oxidation processes, in which, under high moisture conditions, the interaction of impinging light photons with the semiconductor band structure of CdS gives rise to electron-hole pairs, of which the positive holes may cause oxidation of sulfidic ions (S^{II}) to the sulphate (S^{VI}) form [13]. The interpretation of such experimental data is consistent with *ab initio* simulations on the subject [14,15]. However, artificial aging experiments conducted on CdS paint mockups have revealed that such an oxidation can also take place without light, provided a number of conditions are met, namely: (a) an elevated level of relative humidity ($\geq 95\%$) and (b) the presence of cadmium chloride compounds, including $CdCl_2$, $CdCl_2 \cdot nH_2O$ and $Cd(OH)Cl$. Next to the oxidation reaction *per se*, secondary reactions involving dissolution, migration through the paint and recrystallisation of water-soluble phases, such as Na_2SO_4 and $Cd(OH)Cl/CdCl_2$, may further contribute to the formation of cadmium sulfates and of various Cl compounds in the investigated paintings.

The presence of $Cd(OH)Cl$ on the micro scale has been strongly associated with the oxidation of CdS to $CdSO_4$. Evidence was found suggesting that the originally present $Cd(OH)Cl$ particles dissolved, migrated, and recrystallized as nanoparticles, possibly simultaneously with the oxidation of CdS to $CdSO_4$. However, whether the presence of $Cd(OH)Cl$ effectively stimulates the oxidation process is not clear. Does its presence cause/facilitate the oxidation, even in the absence of light, or is its recrystallisation an (after)effect of the oxidative transformation of hex-CdS to $CdSO_4$?

To investigate this question more in detail, a combination of experimental and computational studies of the properties of oil paints made up of both hex-CdS and $Cd(OH)Cl$ was conducted.

The experimental investigation was aimed at documenting the degree of intermixing of both phases at the micro and nanoscale and was conducted using a combination of scanning transmission electron microscopy using energy-dispersive X-ray (STEM-EDX) and synchrotron radiation (SR)-based X-ray techniques of paints prepared from commercially available hex-CdS and a historical early 20th C. cadmium yellow pigment powder before and after artificial aging under high moisture conditions (see

Experimental Section for details). The theoretical investigation, based on density functional theory (DFT) calculations, focused on obtaining new insights about the band alignment and possible charge transfers at the interface between either hex-CdS or cub-CdS on the one hand and CdCl₂ or Cd(OH)Cl on the other hand.

In what follows we first describe a number of experimental results that provide complementary views of the same phenomenon; by combining these, it has become possible to improve our insight regarding the influence of Cd(OH)Cl on the stability of hex-CdS towards oxidation under the influence or in the absence of light.

2. Results and Discussion

2.1 Presence of Cd(OH)Cl and Degradation State of Yellow Paint in Munch's *The Scream* (ca. 1910)

In Fig. 1, a summary is presented of the micro X-ray fluorescence (μ -XRF) images and micro X-ray absorption near edge structure (μ -XANES) spectra and derived from a paint scraping sample of *The Scream* (ca. 1910) by E. Munch. As evident from these data, it concerns a CdS-containing yellow paint microflake. Colocalized with Cd and S there are abundant amounts of Cl, with sulfate-compounds present as micrometric agglomerates (Fig. 1B,C). The latter consist of Na₂SO₄ (i.e., a residue of the CdS synthesis) along with a variable contribution of CdSO₄ and sulfite (S^{IV})-compounds, as revealed by S K-edge μ -XANES spectroscopy measurements (Fig. 1D, leftmost panel). The Cl K-edge μ -XANES spectra (Fig. 1D, rightmost panel) show a typically double-peak signature that resembles that of Cd(OH)Cl (pts. 03_{Cl}-04_{Cl}), although the broadening of the XANES feature at observed at 2.8262 keV (pts. 01_{Cl}-02_{Cl}) also suggest that Cl is present in one or more other compounds. As reported elsewhere ^[8], similar observations were made from other paint fragments of this painting.

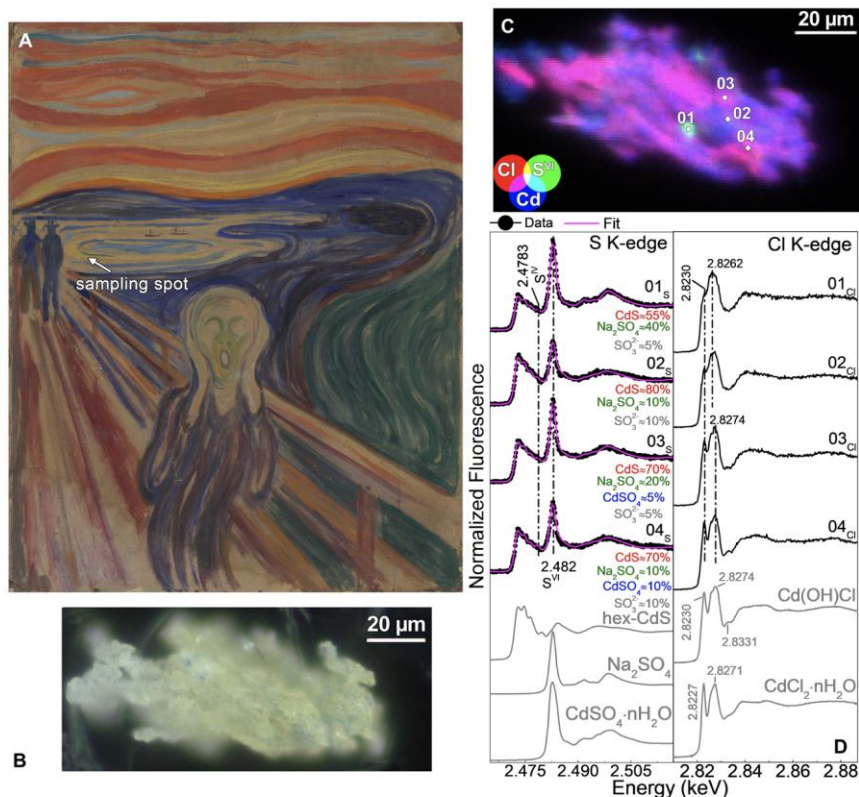


Figure 1. (A) Photograph of *The Scream* (ca. 1910) (MUNCH Museum, Oslo; catalog no. Woll.M.896) with arrow showing the spot where the microflake sample of (B) was taken off (Photo credit: Irina Crina Anca Sandu and Eva Storevik Tveit, MUNCH Museum, Oslo). (B) Visible light micrograph of the studied microflake and corresponding. (C) Composite RGB SR μ -XRF maps of Cl/S^{VI}/Cd (step size: $0.8 \times 0.8 \mu\text{m}^2$, exp. time: 100 ms/pixel). (D) Selection of (left) S K-edge and (right) Cl K-edge μ -XANES spectra (black) obtained from the areas shown in (C). In magenta, result of the linear combination fitting of different S-based compounds, while in grey spectra of a series of S and Cd reference compounds.

2.2 Paint Micro/Nanostructure as Observed by STEM-EDX

Figs. 2-3 illustrate the high-angle annular dark-field (HAADF) images and elemental STEM-EDX maps derived from the two paint mock-ups shown in Figs. 4A-5A and with composition very similar to the microflake of *the Scream* (ca. 1910) (see SI for details about the paints preparation and analysis).

In the $\text{CdS}_{\text{Cd}(\text{OH})\text{Cl}}$ paint (Fig. 2), the distributions of S and Cd, O and C at the nanoscale are essentially complementary to each other. Well-defined hex-CdS grains of dimensions $>1 \mu\text{m}$ are visible within the organic paint matrix; at some locations, they are interspersed with finer and more

irregularly shaped Cd(OH)Cl particles. Low amounts of Cl are present in the sample support, probably as contaminant.

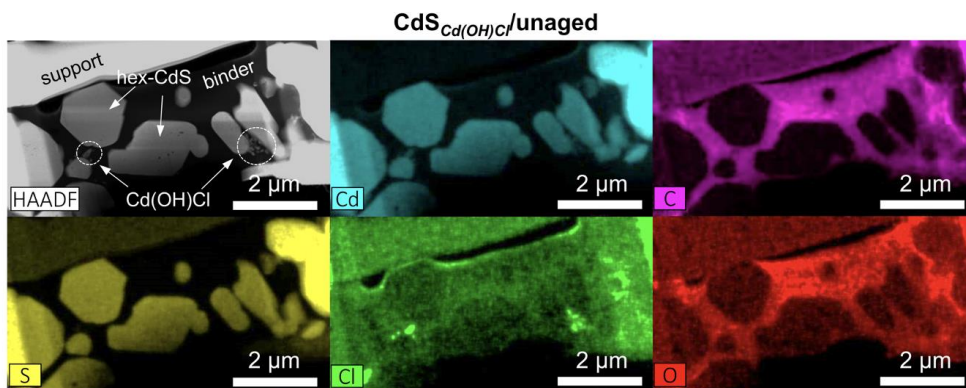


Figure 2. STEM-HAADF image and STEM-EDX maps (Cd-L, C-K, S-K, Cl-K, O-K) of the unaged $\text{CdS}_{\text{Cd(OH)Cl}}$ mock-up paint prepared as thin section by focused ion beam (FIB) (see Figure S2 to see the results obtained from the corresponding aged sample).

When comparing the maps collected from 7914 $_{\text{Cd(OH)Cl}}$ paint (Fig. 3), the smaller average size and irregular shape of the grains is evident. Locations/nanograins are identifiable in which Cd, S and Cl are all present together, while also several grains containing Cd, but neither S and Cl are visible (corresponding to CdCO_3 – C and O). Together with the available XRD data (not reported; see Ref.^[8] for details), showing clearly defined and unbroadened patterns of hex-CdS and Cd(OH)Cl, these nano-level maps suggest that in 7914 $_{\text{Cd(OH)Cl}}$ paint, hex-CdS and Cd(OH)Cl are intimately intermixed with each other, but at a level that still preserves, in part or in total, the crystal structure of both components. The simultaneous presence of an amorphous mixed phase of both components can also not be excluded. The widespread presence of C and O in the surrounding areas the Cd-based particles is due to the oily binder. A more detailed view of the intimate mixture of hex-CdS, Cd(OH)Cl and other compounds, such as CdCO_3 , that is present in sample 7914 $_{\text{Cd(OH)Cl}}$ is provided in Fig. S1.

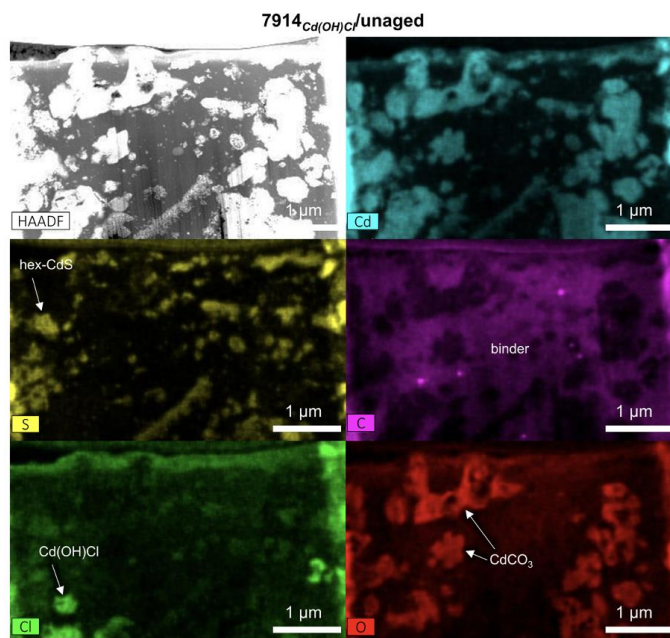


Figure 3. STEM-HAADF image and STEM-EDX maps (Cd-L, C-K, S-K, Cl-K, O-K) of the unaged 7914_{Cd(OH)Cl} mock-up paint prepared as thin section by focused ion beam (FIB) (see Figures S1 and S3 for a detailed map acquired from a cluster of nanograins in the sample and the results obtained from the corresponding aged paint).

From the above-described maps it can be concluded that in the mixtures, also at the nanoscale, the two materials co-exist next to each other as a simple mixture. This essentially remains the same after thermal aging (Fig. S2-S3).

2.3. Effects of Thermal Aging

In Figs. 4A and 5A, photographs of the two paint mock-ups studied with STEM-EDX in the previous section, are presented, before and after aging. As a result of the thermal treatment, the visual aspect of both 7914_{Cd(OH)Cl} and CdS_{Cd(OH)Cl} show an appreciable color change poorly appreciable with the naked eye, along with the formation of superficial whitish-transparent spots.

This macroscopic observation can be linked to several chemical changes that are apparent at the microscopic level.

In line with previous measurements performed in an equivalent thermally aged mock-up^[8], high moisture conditions promotes the formation of S^{VI}-rich aggregates within the S^{II}-based matrix in the 7419_{Cd(OH)Cl} paint (Fig. 4B). S K-edge XANES measurements (Fig. 4C, leftmost panel) reveal that the aggregates mainly consisting of CdSO₄/CdSO₄·nH₂O, while lower amounts of the same compounds are present in the CdS-based matrix. In the aggregate also some evidence of the presence of sulfite (S^{IV}) species was encountered. In addition, the colocalized presence of Cl species and cadmium sulfates was noted: Cd(OH)Cl was mainly localized in the S^{VI}-rich aggregates that formed *in situ* during aging. Earlier μ-XRD patterns recorded from S^{VI}-rich region^[8] show an extensive broadening of the Cd(OH)Cl signals compared to those of sample 7914 before thermal aging, assumed to stem from the nanometric size (>10 nm) of the Cd(OH)Cl crystals. This observation, integrated with the nanoscale maps (Fig. S3) showing both colocalization and in some cases a Cl-rich or CdCO₃ coating covers a Cd,S-rich core, suggests that a recrystallisation of Cd(OH)Cl and possibly of CdCO₃ occurs as part of the aging process.

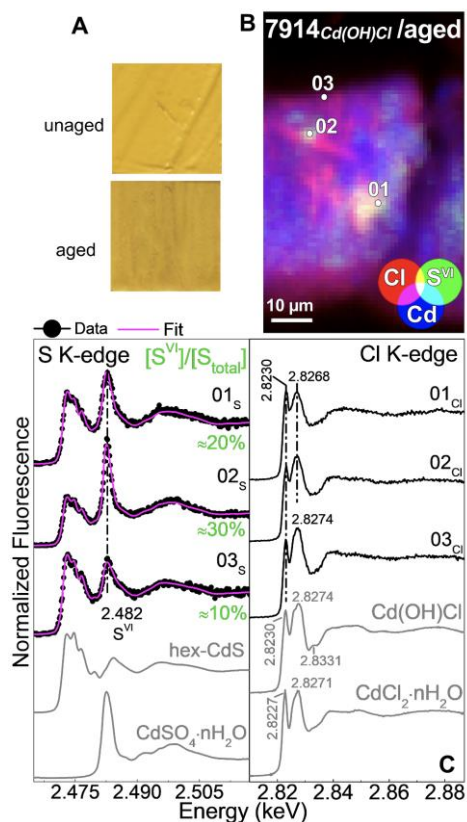


Figure 4. Summary of μ -XRF and μ -XANES investigations of thermally aged 7914 $_{Cd(OH)Cl}$ paint mock-up (RH \geq 95%, T=40°C, 100 days) shown in (A). (B) Composite RGB μ -XRF images of Cl/S^{VI}/Cd [step size (h \times v): 1 \times 1 μ m², exp. time: 100 ms/pixel] and (C) selection of S K-edge and Cl K-edge μ -XANES spectra (black) obtained from the points indicated in (B) with linear combination fitting results (magenta).

Comparable results were also observed for the CdS $_{Cd(OH)Cl}$ paint. Before aging (Fig. S4), SR μ -XRF mapping, S- and Cl-speciation investigations reveal that Cd(OH)Cl particles/aggregates are homogeneously distributed within the yellow paint, where only S^{-II}-species (CdS) were found. As a consequence of the thermal treatment, SR μ -XRF maps (Fig. 5B,D) show that the whitish regions of the paint are mainly composed of Cd and Cl with minor abundances of S. More specifically, the S-speciation maps (Fig. 5E) combined with the linear combination fitting of S K-edge μ -XANES spectra (Fig. 5F, pt 03_s) and SR μ -XRD mapping (Fig. 5C) reveals the formation of CdSO₄ (\approx 20%) in the Cd(OH)Cl/CdCl₂·H₂O-rich area at the surface,

whereas only hex-CdS is present in the Cl-free/poorest regions underneath. CdSO₄ was not revealed by μ -XRD, likely due to its amorphous nature.

The above observations, in combination with the fact that the formation of neither CdSO₄ nor cadmium carboxylates was observed in Cl-free CdS oil paint mock-ups aged under similar conditions [13], led to the conclusion that, in a moist environment, the close contact of Cd(OH)Cl [and possibly other (Cd,Cl) compounds] with hex-CdS particles stimulates the degradation of CdS oil paints. On the other hand, the photodegradation of CdS did not appear to be influenced by the absence or presence of (Cd,Cl) compounds but only by humidity.

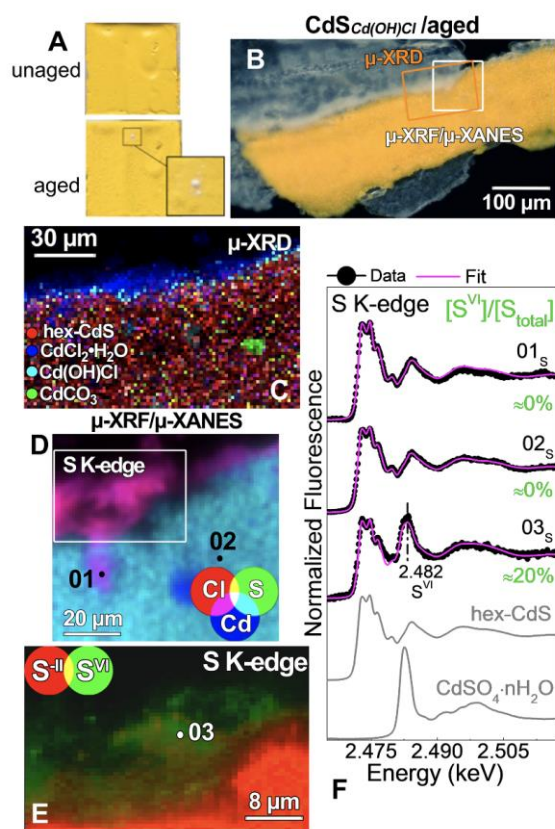


Figure 5. Summary of μ -XRD, μ -XRF and μ -XANES analysis of the thermally aged CdS_{Cd(OH)Cl} mock-up (RH \geq 95%, T=40°C, 100 days) shown in (A, B). (C) Composite RGB SR μ -XRD maps of hex-CdS/CdCl₂·H₂O/Cd(OH)Cl (step size: 1.5 \times 1.5 μ m², exp. time: 1s/pixel, energy: 21 keV) and μ -XRF images of (B,F) Cl/S/Cd and (G) S^{II}/S^{VI} [step size (h \times v): 0.8-1 \times 0.5-1 μ m², exp. time: 80-100 ms/pixel]. In (B), the areas where maps of (C-E) were acquired are shown. (F) Selection of S K-edge μ -XANES spectra (black) obtained from the points indicated in (D,E) and linear combination fitting results (magenta).

2.4 Prediction of Electron Transfers between CdS and Cd(OH)Cl

Since no experimental observations can be done at the level of the individual atoms of the interfacial region between CdS and Cd(OH)Cl a series of theoretical calculations were undertaken to study the possible flow of charges between the two phases. Previously, DFT calculations were performed on CdS and related systems ^[14,15]. In this paper, we perform DFT calculations for CdS, CdCl₂ and Cd(OH)Cl by using the Vienna Ab initio Simulation Package (VASP)^[16-19] with Perdew-Burke-Ernzerhof (PBE) functional^[20]; the computational details of the calculations are given in the Section 5.

2.4.1 PBE Lattice Parameter Calculations with(out) van der Waals Correction

The purpose of these calculations was to determine the atomic positions in cub-CdS, hex-CdS, CdCl₂ and Cd(OH)Cl corresponding to a minimal overall energy of the structures and to verify that the calculated values match experimental data. In Table 1, experimental and calculated lattice

Table 1. Experimental (exp) and calculated values (PBE) for the lattice parameters of cub-CdS, hex-CdS, CdCl₂ and Cd(OH)Cl structures. Experimental values were obtained from References ^[21-23]. For CdCl₂ and Cd(OH)Cl, the lattice parameters are shown with and without Van der Waals (vdW) correction.

	$a^{\text{exp}}(\text{Å})$	$a^{\text{PBE}}(\text{Å})$	$c^{\text{exp}}(\text{Å})$	$c^{\text{PBE}}(\text{Å})$
cub-CdS	5.818	5.936	5.818	5.936
hex-CdS	4.137	4.201	6.716	6.847
CdCl₂	3.864		17.576	
with vdW		3.824		17.757
without vdW		3.909		19.535
Cd(OH)Cl	3.665		10.231	
with vdW		3.672		10.357
without vdW		3.727		10.613

parameters of these compounds are compared. For both CdS polymorphs a good match between calculations and experiment is obtained. For the CdCl₂ and Cd(OH)Cl, the calculated lattice constants also agree well with experiment provided the calculations are done with a Van der Waals (vdW) correction. This illustrates the importance of including these corrections in the calculations.

2.4.2 Band Alignment Calculations

The purpose of band alignment calculations is to assess in which direction electrons and/or positive holes, created in one of the phases (e.g., Cd(OH)Cl) might flow to another phase in contact with it (e.g., cub-CdS or CdCl₂). From the band alignment calculations, values for the ionization energies (IE) and electron affinities (EA) of the various compounds were obtained, and listed in Table 2. In all cases, these are in agreement with literature values ^[24].

Table 2. PBE calculation results for the ionization energy (IE) and electron affinity (EA) for the various slab structures, and the value of the work function of a 1 layer and 12 layer Cd(OH)Cl slab structure.

	IE (eV)	EA (eV)	Work function (eV)
cub-CdS	6.00	4.70	-
hex-CdS	5.96	4.72	-
CdCl₂	7.94	4.38	-
1 layer			
Cd(OH)Cl			
OH site	4.13	1.74	-
Cl site	7.89	5.50	-
12 layer			
Cd(OH)Cl			
OH site	-	-	2.25
Cl site	-	-	8.00

In what follows the electronic structure of the layered compound Cd(OH)Cl is discussed. In the calculations, we considered slabs with the natural (0001) polar surface. Because of this polar nature of Cd(OH)Cl, a potential difference exists between the bottom and top surface of the slabs, creating a built-in dipole perpendicular to the surface of the slab. This potential difference leads to a shift in the vacuum levels between both sides of the slab.

To investigate the influence of the thickness of the Cd(OH)Cl slab on this difference in vacuum levels, we first considered a single layer of Cd(OH)Cl. Fig. 6 shows the crystal structure of single layer Cd(OH)Cl slab. In the layer of Cd(OH)Cl, there is a Cl-Cd-O-H atomic arrangement along the z-axis, which is perpendicular to the layer, and it has two different terminations (OH on one side and Cl on the other side).

Its density of states (DOS) is shown in Fig. 6, indicating that such a single Cd(OH)Cl layer features a clear band gap. Thus, without external excitation (via absorption of photons), no charge carriers can flow across this layer between both outer surfaces that otherwise would reduce the magnitude of the above-mentioned dipole. However, when more layers are added, the electronic structure changes and the system evolves from a semiconductor into a semimetal, with increased conductivity of the material. This is presented in Fig. 7, which shows the density of states per layer for a 12 layer Cd(OH)Cl slab. The metallicity is visible in the DOS of layers 1 (OH-terminated surface) and 2 and of layers 11 and 12 (Cl-terminated surface), which therefore should have the ability to conduct charges along the surface of the slab, i.e. parallel to the direction of the slab. If we consider the DOS of the other layers, they show a band gap and thus retain their semiconductor nature. The above-mentioned conductivity therefore will be not present in the direction perpendicular to the slab without external excitation. We also see in Fig. 7A that the positions of the valence band maximum (VBM) and the conduction band minimum (CBM) shift to higher energies when moving from layer 1 (OH-terminated surface) to layer 12 (Cl-terminated surface).

Since the VBM of layer 12 lies above the CBM of layer 1, upon (photo or thermal) excitation of the system, a net charge transfer is expected to occur between both surfaces, creating a reservoir of positive holes (a hole pocket) at the Cl-terminated side of Cd(OH)Cl and an reservoir of electrons (an electron pocket) at the OH-terminated side. This charge transfer compensates to a certain extent for the built-in dipole in Cd(OH)Cl. The planar-averaged local potential energy along the direction perpendicular to the slab for this 12 layer Cd(OH)Cl slab is shown in Fig. 7B. Here we can see that even after the charge transfer, an internal dipole perpendicular to the slab surfaces remains. This indicates that the charge transfer is not able to compensate completely for the built-in electric field.

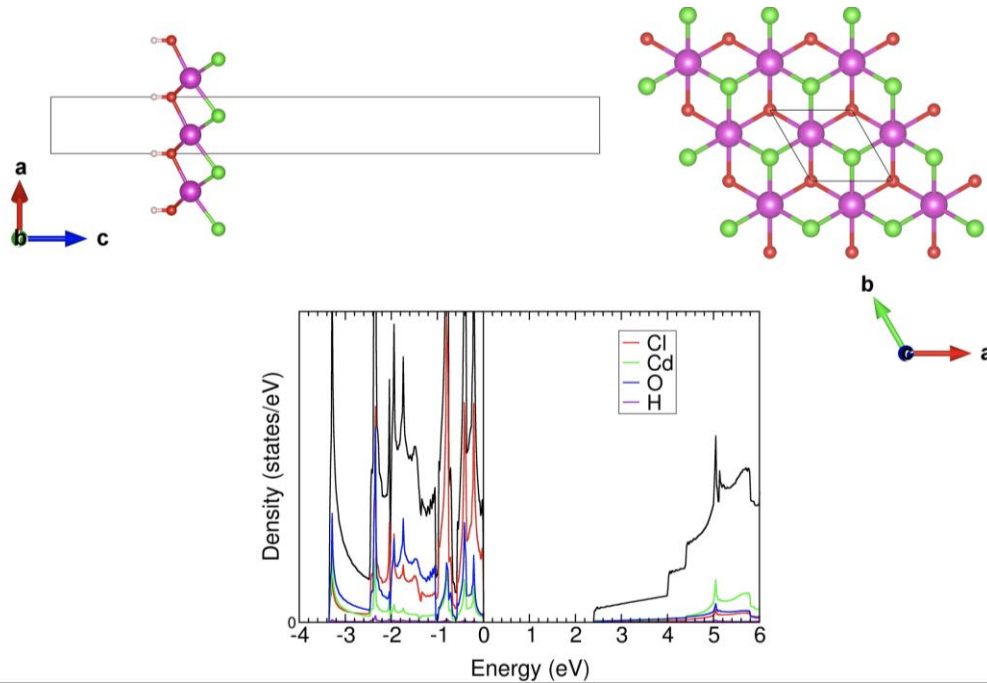


Figure 6.

The top left figure shows the side view and the top right figure shows the top view of the crystal structure of 1 layer Cd(OH)Cl, respectively. Here, atom color codes: green: Cl; pink: Cd; red: O; white: H atoms. The bottom figure shows the density of states (DOS) for 1 layer Cd(OH)Cl. Here, the red is Cl, the green is Cd, the blue is O and the purple is H. Black line shows the total DOS. Black vertical line shows the Fermi level and it was set to 0 eV. Energies are given with respect to the top of the valence band.

The energy difference between the vacuum levels at the OH-terminated and Cl-terminated side of Cd(OH)Cl with respect to the number of layers is shown in Fig. 7C. For the metallic systems, this corresponds to the difference in work functions between both sides. The IE and EA values for the Cd(OH)Cl monolayer and the work function values for the thicker Cd(OH)Cl slabs at both the OH- and Cl-terminated Cd(OH)Cl surfaces are included in Table 2. As shown in Fig. 7C, the

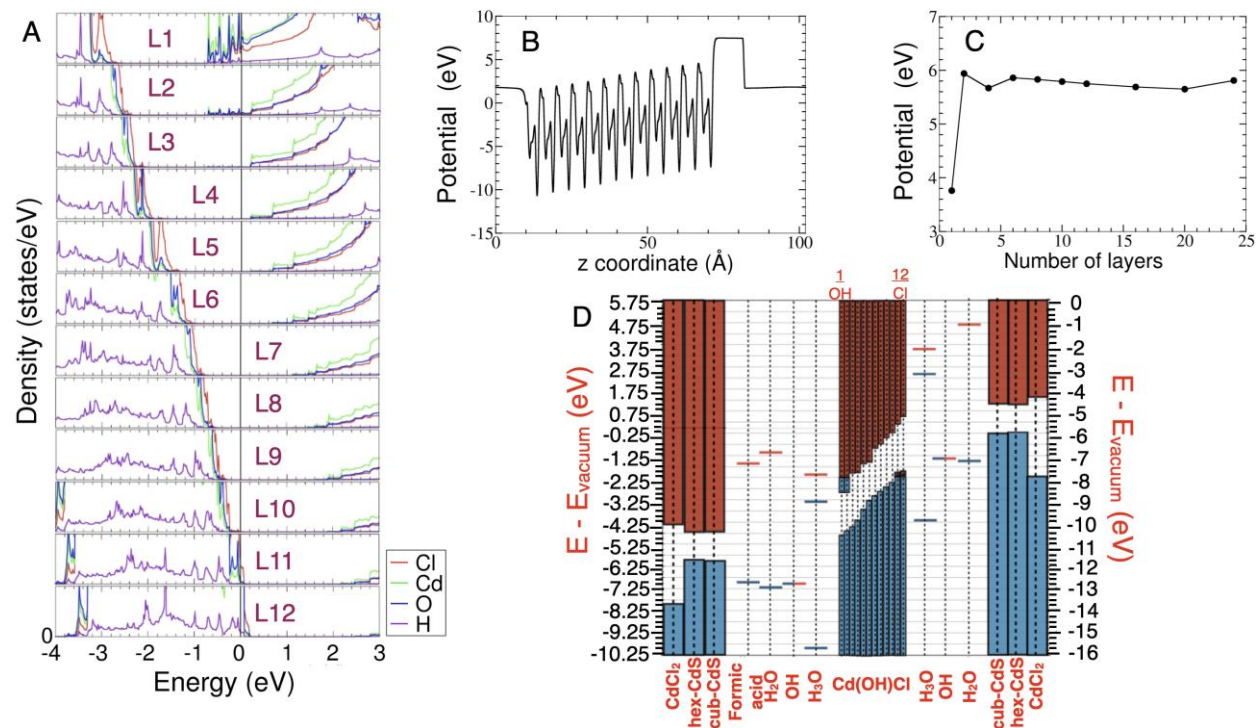


Figure 7. A) Density of states (DOS) for a slab consisting of 12 layers of Cd(OH)Cl. Here the black vertical line shows the Fermi level and it was set to 0 eV. Energies are given with respect to the top of the valence band. Layer 1 (L1) is the OH-terminated and layer 12 (L12) is the Cl-terminated surface of the slab. B) Average local potential for a bare Cd(OH)Cl slab along the direction perpendicular to the surface (z). C) Potential difference between the vacuum levels at the two surfaces of Cd(OH)Cl as a function of slab thickness/number of layers. The potential difference converges to approximately 5.8 eV. D) Band alignment diagram of Cd(OH)Cl in contact with other materials. Blue blocks and red blocks represent the valence band (VB) and conduction band (CB) of solid material slab with respect to the vacuum level, respectively. Blue horizontal lines represent the highest occupied molecular orbitals (HOMO) of molecules in contact with the Cd(OH)Cl slab surfaces; red horizontal lines are the lowest unoccupied molecular orbital (LUMO) of these molecules. Half blue-half red lines are partially filled electronic states of these molecules. Next to values for the neutral molecules water and formic acid, also values for the H₃O and OH radicals are indicated.

energy difference between the two surfaces of Cd(OH)Cl bilayer is approximately 6 eV, close to the approximate value reported in Ref [25]. Note that with increasing slab thickness, this energy difference converges to a value of around 5.8 eV and becomes independent of the slab thickness. To explain this observation, we present a simple charge transfer model for Cd(OH)Cl in Section 3 of Supporting Information.

2.4.3 Band Alignment Diagram of Cd(OH)Cl in contact with Various Other Materials

Based on the obtained EA, IE and work functions, the band alignment diagram shown in Fig. 7D is proposed. In this diagram we consider which charge transfers might occur when both surfaces of a central slab of Cd(OH)Cl would be in contact with various other materials: (a) either solid slabs of hex-CdS, cub-CdS or CdCl₂ or (b) individual molecules directly in contact with both surfaces. For the latter we considered water (H₂O) as well as the H₃O and OH radicals, and formic acid (HCOOH) of which both the highest occupied molecular orbital (HOMO) and lowest unoccupied molecular orbital (LUMO) levels are considered.

In Fig. 7D, for the solid slabs, the calculated positions of the valence band (VB) and conduction band (CB) are indicated by blue and red blocks, respectively. All these positions were obtained by aligning the vacuum levels. The dipole across the central Cd(OH)Cl slab, causes the VBM and CBM values for the materials in contact with the Cl-terminated surface of the central Cd(OH)Cl slab (right side of Fig. 7D) to be shifted to lower potentials while those in contact with OH-terminated surface (left side of Fig. 7D) are shifted upwards. For the molecules and radicals, the blue horizontal lines indicate the (shifted) HOMO level and the red horizontal lines the (shifted) LUMO level, half blue-half red lines represent partially filled electronic states. The DFT calculations to obtain the HOMO and LUMO levels were done for bare radicals.

It is important to note that this band alignment diagram illustrates the situation (just) before the different slabs and molecules are brought into contact with each other, i.e., provides indications in which direction electrons and/or positive holes might move among the various materials before they actually move.

2.4.4 Bader Charge Analysis

In order to check the consistency of the above-described mechanism, we performed Bader charge analysis ^[26,27] for two different systems. One system is the Cd(OH)Cl slab in contact with

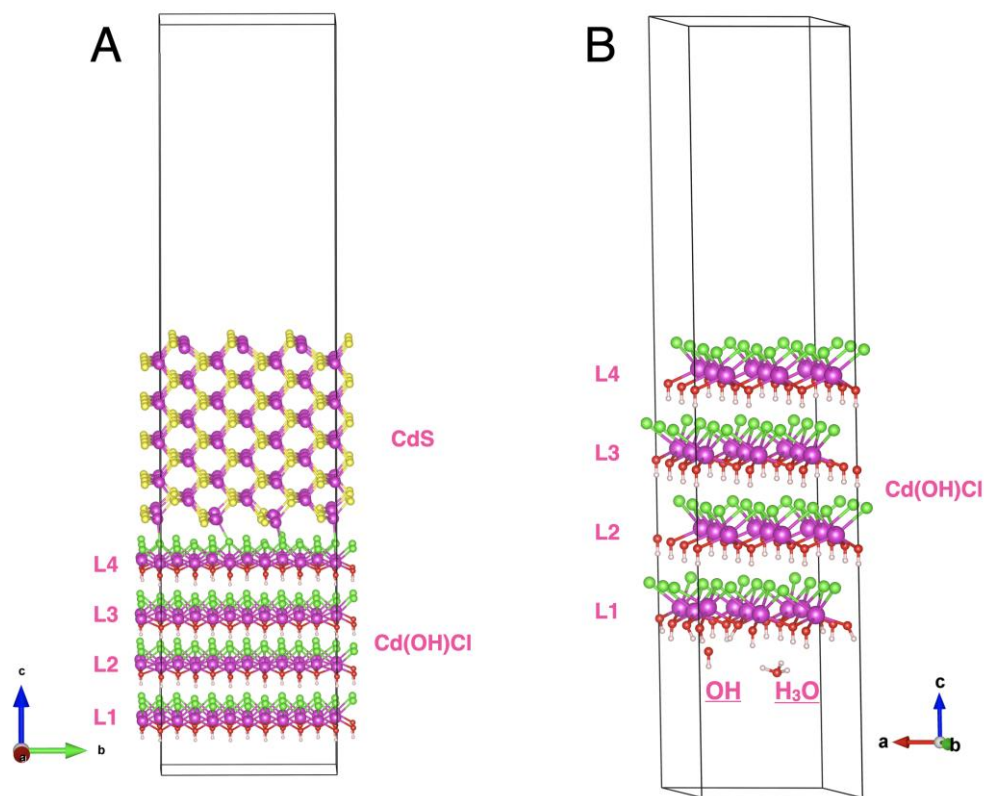


Figure 8. A) Cd(OH)Cl slab in contact with CdS on its Cl-side. The total system was constructed from a 2x5 supercell of 4 Cd(OH)Cl layers and a 3x3 supercell of cub-CdS with 10 atomic layers. B) Cd(OH)Cl slab with ·OH and H₃O· radicals adsorbed on its OH-side. Here a 2x2 supercell of 4 Cd(OH)Cl layers was used. Here L1, L2, L3 and L4 show the Layer 1-4 of Cd(OH)Cl. (Atom color codes: pink: Cd; yellow: S; green: Cl; red: O; white: H atoms).

a CdS slab on its Cl side (anodic side) and the other system is the Cd(OH)Cl slab with $\cdot\text{OH}$ and $\text{H}_3\text{O}\cdot$ radicals adsorbed on its OH-side (cathodic side). Fig. 8A shows the situation in which CdS is in contact with the Cl layer. Here we observe a covalent bond between CdS and the Cl layer of Cd(OH)Cl. Fig. 8B shows the $\cdot\text{OH}$ and $\text{H}_3\text{O}\cdot$ radicals at the OH layer Cd(OH)Cl.

Table 3 shows the Bader charge analysis of the different layers in a 4-layer Cd(OH)Cl slab. Column 1 shows the Bader charge analysis of a bare Cd(OH)Cl slab (i.e. no adsorbed molecules or direct contact with CdS). If there was no electron transfer between the layers, the total electron number of each layer would be equal 26 (as layer 2 and 3). However, the results show that a charge

Table 3. Bader charges (in units of the elementary charge e) of the different layers in a 4 layered Cd(OH)Cl slab. Column 1 shows the results for bare (no molecules or CdS in contact with the slab) Cd(OH)Cl. The results in column 2 are for CdS in contact with Cd(OH)Cl at the Cl-terminated side, and column 3 shows the results for $\text{H}_3\text{O}\cdot$ and $\cdot\text{OH}$ adsorbed on the OH-terminated side of Cd(OH)Cl. Here layer 1 is OH-terminated side of Cd(OH)Cl and layer 4 is the Cl-terminated side of Cd(OH)Cl.

	bare Cd(OH)Cl	Cd(OH)Cl with CdS at Cl-side	Cd(OH)Cl with $\text{H}_3\text{O}\cdot$ and $\cdot\text{OH}$ at OH-side
Layer 1 (OH)	26.13	26.13	26.07
Layer 2	26.00	26.00	26.00
Layer 3	26.00	26.00	26.00
Layer 4 (Cl)	25.86	25.97	25.86

of approximately $0.13 e$ is transferred from layer 4 (the Cl-terminated side) to layer 1 (the OH-terminated side). The second column shows the results for Cd(OH)Cl with CdS at its Cl-side. In these calculations the CdS structure is fully relaxed. Here we can see that the charge in layer 4 increases approximately by $0.1 e$, which shows that electrons from the valence band of CdS flow towards the Cl-terminated surface. The third column of Table 3 shows the Bader charges of all

layers after the adsorption of $\cdot\text{OH}$ and H_3O^+ , obtained after a full relaxation of the system. We can see that after the relaxation, indeed the charge in layer 1 has decreased, as predicted by the band alignment diagram.

The Bader charge analysis is therefore consistent with our proposed mechanism for the oxidation of CdS: the electrons that are extracted on the anodic (Cl-terminated) side of Cd(OH)Cl, causing an oxidation of CdS, are transferred through the Cd(OH)Cl to its cathodic (OH- terminated) side where they are transferred to species such as OH or H_3O^+ .

2.5 Proposed Degradation Mechanism

The above results indicate that Cd(OH)Cl is a polar semimetal with built-in electrical dipole and that the potential difference over the system does not change with slab thickness. In the right side of Fig. 7D we can see what would happen if hex-CdS, cub-CdS or CdCl₂ would be brought into contact with the Cl-terminated (anodic, oxidizing) surface of Cd(OH)Cl: in the case of either hex-CdS or cub-CdS, electrons from the VB of the CdS would flow towards the Cl-terminated surface of the Cd(OH)Cl to fill the hole states that are present there (corresponding to an anodic half reaction). One can conclude a similar manner that also H₂O molecules and OH radicals could act as source of electrons. As such, the Cl-terminated surface of the Cd(OH)Cl slab can be considered to act as anodic surface, with the ability to oxidize some of the components it is in contact with. On the other hand, and consistent with chemical expectations, Figure 7D also shows that when CdCl₂ and the Cl- terminated Cd(OH)Cl surface would make contact, no electron flow would take place.

The left side of Fig. 7D permits to imagine what might take place on the OH-terminated (or cathodic, reducing) surface of the Cd(OH)Cl slab: the electrons present in the CB of Cd(OH)Cl (layers 1 and 2 of the slab) could flow to hole states in either hex-Cd, cub-CdS or CdCl₂ and to

half-filled states of OH radicals (corresponding to cathodic half reaction). The HOMO of small molecules such as water and formic acid, however, are too high in energy to be able to accept such electrons. The same applies to the HOMO of the H₃O radical. The removal of charge from the OH-terminated Cd(OH)Cl surface would thus compensate for the extra electrons present at top of the valence band of the Cl-terminated Cd(OH)Cl surface. The schematic illustration of this process is shown in Fig. 9.

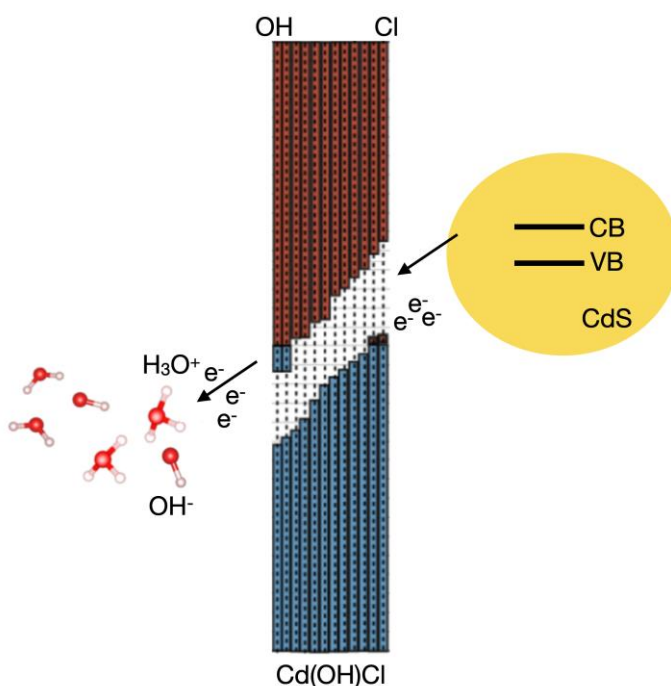
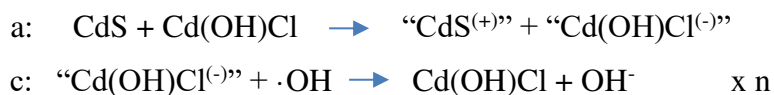


Figure 9. Schematic illustration of the oxidation of CdS. Here, VB is the valence band and CB is the conduction band of CdS. The blue and red blocks represent the valence band and conduction band of Cd(OH)Cl, respectively.

From the above consideration, it is possible to conclude that a slab of Cd(OH)Cl might play a role of charge mediator, extracting electrons from CdS (in contact with its anodic surface) and delivering them to OH radicals (in contact with its cathodic surface), a conversion that might be denoted as follows:





where “Cd(OH)Cl⁽⁻⁾” denotes the slab of Cd(OH)Cl that has acted as electron acceptor on its OH-terminated surface and subsequently play the role of electron donor at its Cl-terminated surface. When n = 8, this equation essentially describes the Cd(OH)Cl-catalyzed oxidation of sulfidic ions (S²⁻, valence state -II) in CdS to sulfate ions (SO₄²⁺, S valence state +VI), and can then also be written as:

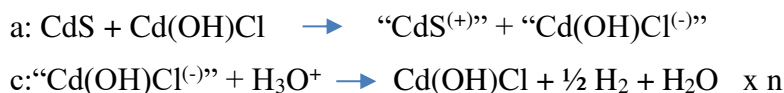


or finally



It is not unreasonable to assume that near the electron-depleted surface of CdS, also water molecules are present of which the O-atoms can interact with the oxidized S atoms to form sulphate (SO₄²⁻) ions.

Since we do not have direct access to the HOMO and LUMO levels of the OH⁻ and H₃O⁺ ions, the calculated HOMO and LUMO energy levels of bare (i.e., unsolvated) H₃O[·] and ·OH radicals were used in the above calculationsⁱ. While it is not possible to quantitatively calculate the H₃O⁺ LUMO level within our supercell approach, the energy level will be lower than the H₃O[·] HOMO level due to the reduced electron repulsion and thus will be situated below the occupied CB states of the OH-terminated Cd(OH)Cl surface (see Fig. 7D). Thus, a charge transfer from the cathodic Cd(OH)Cl surface towards H₃O⁺ could also take place, with the hole states created in the cathodic surface filled by charges extracted from CdS on the anodic side of the Cd(OH)Cl slab. In case H₃O⁺ is the electron sink species, both half reactions become:





or, for $n = 8$:



The above considerations are consistent with the documented ability of CdS to act as a water-splitting photocatalyst, potentially with high hydrogen generation efficiency^[30]. However, an important aspect that limits its effective use for this purpose is that CdS, like other sulfidic materials, is prone to photocorrosion and self-decomposition^[31].

3. Conclusion

On the basis of the experimental and theoretical investigations, it is possible to provide further evidence about the effect that Cd(OH)Cl and moisture have on the tendency of hex-CdS towards oxidation to CdSO₄ in oil paintings. First, Cd(OH)Cl was shown to be mixed on the nanoscale with hex-CdS (and other Cd-compounds) in both original works of art such as Munch's *The Scream* (ca. 1910) and in cadmium yellow paint mock-ups. STEM-EDX map of the mixture indicated that both phases are intergrown at the nanometer level. However, as this mixture still exhibits the distinct and sharp XRD signals of both compounds, we conclude that both phases retain many of the (electronic) properties they have in pure, unmixed form. Nevertheless, at the interface of both materials, material properties may be present that are not exhibited by both components when present in pure form. These properties were studied by means of density functional theory calculations for slabs of CdS, Cd(OH)Cl and CdCl₂.

Due to the presence of a built-in dipole in Cd(OH)Cl, giving rise to superficial layers with metallic properties, thin layers of such compound feature opposed surfaces with respectively anodic and cathodic properties. When in contact with respectively CdS and water, the Cd(OH)Cl can facilitate the transfer of electrons from the sulfidic ions in the vicinity of its anodic surface (CdS/Cd(OH)Cl interface) to either OH radicals or H₃O⁺ ions on its cathodic side, thereby

stimulating the oxidation of CdS to CdSO₄. Thus, Cd(OH)Cl may play the role of a oxidative catalyst for CdS in an aqueous environment. The very intimate intermixing of CdS and Cd(OH)Cl, down to the nm scale, is expected to enhance this behavior.

4. Experimental Section

4.1. The Scream (ca. 1910) (MUNCH Museum, Oslo, Norway) microflake

The paint microflake that was analyzed was obtained from a spot of the flaked-off yellow paint surface of the lake region of The Scream (ca. 1910) (tempera and oil on unprimed cardboard, 83.5 cm by 66 cm; catalog no. Woll.M.896) belonging to the MUNCH Museum ([Figure 1A](#)). It was obtained by scraping the surface, resulting in six discrete micrometric flakes; all of them were directly measured without any further preparation. The results obtained from one of them, representative of the composition of the micro-sampling location, are presented and discussed.

4.2 Preparation of CdS-based paint mock-ups and aging protocol

An oil paint mock-up was prepared by mixing an early 20th century cadmium yellow pigment powder (henceforth referred to as the “7914_{Cd(OH)Cl}” paint) from the collection of the Cultural Heritage Agency of the Netherlands (RCE) with linseed oil (Zecchi) in a 4:1 weight ratio and applied on polycarbonate slices. This powder dates back to the early 20th century and contain CdCO₃, Cd(OH)Cl and KCl next to poorly crystalline hex-CdS (see Refs. ^[8,11] for more details). An additional paint mock-up was obtained by mixing powders of crystalline hex-CdS (Sigma-Aldrich) and Cd(OH)Cl (in-house synthesized, according to the procedure reported in Ref. ^[32]) in a 4:1 weight ratio (above referred to as the “CdS_{Cd(OH)Cl}” paint). A blend of the powder mixture with linseed oil (4:1 weight ratio) was applied on areas of about 1.5 cm by 1.5 cm on a polycarbonate support.

Thermal aging treatment of both paint mock-ups was performed by placing the touch-dried paints in a vessel maintained in the dark at RH \geq 95% (obtained using distilled water) and at 40°C for an overall period of 90 to 100 days (2160 to 2400 hours). As a result of the treatment, at the paint surface of both mock-ups, a color change appreciable with the naked eye along with the formation of whitish-transparent spots were observed (cf. Figs. 4-5).

4.3 Nanoscale investigation by STEM-EDX

Prior to STEM-EDX measurement, CdS-based oil paint mock-ups were thinned via Thermo Fisher Helios Focused Ion beam (FIB) to a thickness of ca 100 nm and loaded on to a FIB lift-out grid. The STEM-EDX measurements were performed using a Thermofisher Scientific Titan 60-300 kV transmission electron microscope operated at 300 kV and equipped with a super X EDS detector. EDX maps were acquired in STEM mode with a probe current of \sim 200 pA. A beam convergence angle of 21 mrad was used. A parent STEM-HAADF image was acquired at 512 \times 512 pixel resolution and the final STEM-EDX maps were recorded as sub-areas within this image. A pixel dwell time of 10 μ s was used.

4.4 Microscale investigations by μ -XANES/ μ -XRF and μ -XRD

The Scream (ca. 1910) yellow microflake and oil paint mock-ups were examined by means of μ -XANES/ μ -XRF and μ -XRD as here below described.

4.4.1 μ -XANES/ μ -XRF at S K-edge and Cl K-edge

Sulfur and chlorine speciation investigations of a paint microflake obtained from The Scream (ca. 1910) and thin sections (5 to 10 μ m in thickness) of oil paint mock-ups were performed at the

scanning X-ray microscope end station hosted at the X-ray Microscope Beamline ID21 of the European Synchrotron Radiation Facility (ESRF, Grenoble, France) [33]. Investigations were carried out by means of a fixed exit double-crystal Si(111) monochromator and with an incident beam focused with Kirkpatrick-Baez mirrors (KB) down to a diameter of $0.6 \times 0.3 \mu\text{m}^2$ ($h \times v$). The energy calibration was performed using $\text{CaSO}_4 \cdot 2\text{H}_2\text{O}$ and NaCl as standards and by setting the position of the peak maximum of their first-order derivative spectrum at 2.4829 and 2.8261 keV, respectively. XRF signals were collected at 69° with respect to the incident beam direction by means of a single energy-dispersive silicon drift detector (Xflash 5100, Bruker).

Single-point μ -XANES spectra were acquired in XRF mode by scanning the primary energy across the K-edge of S (2.46 to 2.53 keV; energy step, 0.18 eV) and Cl (2.79 to 2.89 keV; energy step, 0.25 eV). The normalization and the linear combination fitting of the spectra against a library of XANES spectra of S, Cl, and Cd reference compounds were performed by means of the ATHENA software [34]. The linear combination fitting (LCF) permitted to quantitatively determine the average relative amount of sulfate (S^{VI}), sulfite (S^{IV}), and sulfide ($\text{S}^{\text{-II}}$) compounds (expressed as $\%[\text{S}^{\text{VI}}]/[\text{S}_{\text{total}}]$, $\%[\text{S}^{\text{IV}}]/[\text{S}_{\text{total}}]$, and $\%[\text{S}^{\text{-II}}]/[\text{S}_{\text{total}}]$) and of different Cd and Cl compounds. Since the well-known sensitivity of pigments and other components of the paints under the exposure to SR X-ray micro-probes [35-38] care was taken to ensure that spectra were not affected from the measurement process.

μ -XRF mapping measurements were performed by employing a monochromatic primary beam of fixed energy at the S K- and Cd L₃-edges. Maps of the same region of interest were acquired using either 80 or 100 ms per pixel at the following energies: (i) 2.473 and 2.482 keV to promote the excitation of sulfides and sulfates, respectively, and (ii) 3.7 keV to obtain the XRF intensity of all S, Cl, and Cd species. The software PyMca [39] was used to fit the XRF spectra and to separate

the contribution of different elements. The experimental procedure used for recording and producing the sulfide and sulfate oxidation state maps according to earlier research [6].

4.4.2 μ -XRD

Thin sections of the CdS-based oil paint mock-ups were investigated at the microprobe hutch of the Hard X-ray Micro/Nanoprobe beamline P06 of the PETRA III storage ring (DESY, Hamburg) [40]. An incident energy of 21 keV was selected by means of a Si(111) crystal monochromator and focused by a KB mirror system down to a diameter of around $0.7 \times 0.7 \mu\text{m}^2$ ($h \times v$). XRD signals were recorded in transmission geometry using a PILATUS 300K area detector. XRD patterns were acquired with 1 s per pixel and calibrated using a LaB₆ reference sample. Crystalline phase distribution maps were obtained by full pattern refinement using the XRDUA software package [41].

5. Density functional theory calculations

In order to understand the oxidation mechanism of CdS to CdSO₄ and the influence of humidity and chlorine-compounds on this process, we studied the electronic properties of CdS and the compounds CdCl₂ and Cd(OH)Cl with density functional theory (DFT)[42,43]. The DFT calculations were performed using the plane-wave basis set and projector augmented-wave (PAW) method [44,45], as implemented in the Vienna Ab-Initio Simulation Package (VASP)[16-19]. In these calculations the Perdew-Burke-Ernzerhof (PBE) functional[20] was used. Because CdCl₂ and Cd(OH)Cl are van der Waals (vdW) layered structures, vdW corrections were included in these calculations by using the DFT-D2 method of Grimme[46]. The energy cutoff was set to 500 eV for the plane-wave basis set. The bulk structures of hexagonal CdS (hex-CdS) and cubic

CdS (cub-CdS) were taken from^[11] and the bulk structures of CdCl₂ and Cd(OH)Cl from Springer Materials^[21].

In order to study the band alignment between CdS and CdCl₂ or Cd(OH)Cl, we performed DFT calculations for the slab structures as shown in Figure S5(A-D) in the Supporting Information. The relative positions of the valence band maximum (VBM), conduction band minimum (CBM) and the vacuum level of CdS, Cd(OH)Cl and CdCl₂ slabs were constructed by employing up to 10 atomic layers for cub-CdS and 12 atomic layers for hex-CdS, 18 atomic layers for CdCl₂ and 48 atomic layers for Cd(OH)Cl. For CdS, the zincblende (with a (110) surface orientation) as well as the wurtzite (with a (101 $\bar{0}$) surface orientation) structure were considered as in^[15, 47]. The two central layers of the slabs were fixed and the remaining layers were relaxed. For the self-consistency calculations, the Brillouin zone was sampled using a Γ -centered 14 \times 14 \times 1 Monkhorst–Pack^[48] k-point grid and the total energy converged to within 10⁻² meV with the force convergence criterion of 0.01 eV/Å. For the density of states calculations, the tetrahedron method with Blöchl corrections^[49] was used and the k-point grid was increased to 28 \times 28 \times 1. Cl 3s² 3p⁵, Cd 4d¹⁰ 5s², O 2s² 2p⁴, H 1s¹ and S 3s² 3p⁴ were treated as valence electrons in all our calculations. We used the standard PAW potentials with the labels Cl, Cd, O and H. In addition, for these calculations the vacuum distance was set to 20 Å. For all these structures the VBM and CBM were determined relative to the vacuum level. Also, the position of the HOMO and LUMO levels of the \cdot OH and H₃O \cdot radicals were obtained relative to the vacuum level. The molecules were therefore placed in 10 Å x 10 Å x 10 Å box so that no interaction occurs between the molecules in the neighboring cells. By aligning the vacuum level, the band alignment between the different compounds was calculated.

We also performed extra calculations for the Cd(OH)Cl-CdS heterostructure which has 500 atoms with 4 layers of Cd(OH)Cl and 10 layers of cub-CdS. In order to minimize the stress at the

interface a heterostructure was built from a 2x5 supercell of Cd(OH)Cl and 3x3 supercell of cub-CdS. The size of the heterostructure supercell was fixed to that of the 2x5 Cd(OH)Cl. Atomic positions were relaxed. To speed up the calculations, 4x4x1 k-points were used.

In the calculations of the system with Cd(OH)Cl and OH and H₃O radicals, a 4-layered 2x2 supercell of Cd(OH)Cl was used.

ASSOCIATED CONTENT

Supporting Information

The Supporting Information is available free of charge on the ACS Publications website.

Materials and experimental methods, STEM-HAADF, STEM-EX and SR-based X-ray measurements of unaged/aged mock-ups including images, Structures of the slabs and Charge transfer model for Cd(OH)Cl.

Corresponding Author

* email : selma.maydabacaksiz@uantwerpen.be

Author Contributions

BP, DL, JV, CM, AR and KJ contributed to acquisition of funds for this project; the overall design of the investigation was done by KJ, SM, BP, DL, LM and AR with assistance from JV,GF and IS; most of the computational efforts were borne by SM with advice from BP and DL; most measurements were performed by LM, SdM, DK, MC and JG; major contributions to data analysis and curation were undertaken by SM, DK and LM with smaller contributions from all others; the

original draft of the paper was prepared by SM, LM, DL, BP and KJ with comments provided by all authors.

ACKNOWLEDGMENT

The experimental research on cadmium yellow powders/paint mock-ups and *the Scream (ca. 1910)* was financially supported by the European Union research projects IPERION-CH (H2020-INFRAIA-2014-2015, GA no. 654028) and IPERION-HS (H2020-INFRAIA-2019-1, GA no. 871034) and the project AMIS, within the program Dipartimenti di Eccellenza 2018-2022 (funded by MUR and University of Perugia). For the beamtime grants received, the authors thank the ESRF-ID21 beamline (experiment nos. HG64 and HG95), DESY-P06 beamline, a member of the Helmholtz Association HGF (experiment nos. I-20130221 EC and I-20160126 EC), and the project CALIPSOplus under the GA no. 730872 from the EU Framework Programme for Research and Innovation HORIZON 2020. All the staff of the MUNCH Museum (Conservation Department) is acknowledged for their collaboration. The computational resources and services used in this work were provided by the VSC (Flemish Supercomputer Center) and the HPC infrastructure of the University of Antwerp (CalcUA), both funded by the FWO-Vlaanderen and the Flemish Government-department EWI.

REFERENCES

- [1] Mass, J. L.; Opila, R.; Buckley, B.; Cotte, M; Church, J; Mehta, A. The photodegradation of cadmium yellow paints in Henri Matisse's *Le Bonheur de vivre (1905–1906)*. *Appl. Phys. A: Mater. Sci. Process.* **2013**, *111*, 59-68.
- [2] Mass, J; Sedlmair, J; Patterson, C.S.; Carson, D; Buckley, B; Hirschmugl, C. SR-FTIR imaging of the altered cadmium sulfide yellow paints in Henri Matisse's *Le Bonheur de vivre (1905–6)* – examination of visually distinct degradation regions. *Analyst* **2013**, *138*, 6032-6043.

- [3] Voras, Z. E. ; DeGhetaldi, K.; Wiggins, M. B.; Buckley, B.; Baade, B.; Mass, J.L.; Beebe, T.P. ToF–SIMS imaging of molecular-level alteration mechanisms in Le Bonheur de vivre by Henri Matisse. *Appl. Phys. A: Mater. Sci. Process.* **2015**, *121*, 1015-1030.
- [4] Pouyet, E.; Cotte, M.; Fayard, B.; Salome, M.; Meirer, F.; Mehta, A.; Uffelman, E.; Hull, A.; Vanmeert, F.; Kieffer, J. et al. 2D X-ray and FTIR micro-analysis of the degradation of cadmium yellow pigment in paintings of Henri Matisse. *Appl. Phys. A: Mater. Sci. Process.* **2015**, *121*, 967-980.
- [5] Van der Snickt, G.; Janssens, K.; Dik, J.; De Nolf, W.; Vanmeert, F.; Jaroszewicz, J.; Cotte, M.; Falkenberg, G.; Van der Loeff, L. Combined use of Synchrotron Radiation Based Micro-X-ray Fluorescence, Micro-X-ray Diffraction, Micro-X-ray Absorption Near-Edge, and Micro-Fourier Transform Infrared Spectroscopies for Revealing an Alternative Degradation Pathway of the Pigment Cadmium Yellow in a Painting by Van Gogh. *Anal. Chem.* **2012**, *84*, 10221-10228.
- [6] Van der Snickt, G.; Dik, J.; Cotte, M.; Janssens, K.; Jaroszewicz, J.; De Nolf, W.; Groenewegen, J.; Van der Loeff, L. Characterization of a Degraded Cadmium Yellow (CdS) Pigment in an Oil Painting by Means of Synchrotron Radiation Based X-ray Techniques. *Anal. Chem.* **2009**, *81*, 2600-2610.
- [7] Ghirardello, M.; Gonzalez, V.; Monico, L.; Nevin, A.; MacLennan, D.; Patterson, C. S.; Burghammer, M.; Refregiers, M.; Comelli, D.; Cotte, M. Application of Synchrotron Radiation-Based Micro-Analysis on Cadmium Yellows in Pablo Picasso's Femme. *Microsc. Microanal.* **2022**, *28*, 1504-1513.
- [8] Monico, L.; Cartechini, L.; Rosi, F.; Chieli, A.; Grazia, C.; De Meyer, S.; Nuyts, G.; Vanmeert, F.; Janssens, K.; Cotte, M. et al. Probing the chemistry of CdS paints in The Scream by in situ noninvasive spectroscopies and synchrotron radiation x-ray techniques. *Sci. Adv.* **2020**, *6* : eaay3514.
- [9] Fiedler, M. B. I. in *Artist's Pigments: A Handbook of their History and Characteristics, Vol. 1* (Ed.: R. L. Feller), Archetype Publications, London, National Gallery of Art, Washington, **1986**, pp. 65-108.
- [10] Ghirardello, M.; Otero, V.; Comelli, D.; Toniolo, L.; Dellasega, D.; Nesi, L.; Cantoni, M.; Valentini, G.; Nevin, A.; João Melo, M. An investigation into the synthesis of cadmium sulfide pigments for a better understanding of their reactivity in artworks. *Dyes Pigm.* **2021**, *186*, 108998.

- [11] Rosi, F.; Grazia, C.; Gabrieli, F.; Romani, A.; Paolantoni, M.; Vivani, R.; Brunetti, B.G.; Colombari, P.; Miliani, C. UV-Vis-NIR and micro Raman spectroscopies for the non destructive identification of $\text{Cd}_{1-x}\text{Zn}_x\text{S}$ solid solutions in cadmium yellow pigments. *Microchem. J.* 2016, **124**, 856-867.
- [12] Milligan, W.O. The Color and Crystal Structure of Precipitated Cadmium Sulfide. *The Journal of Physical Chemistry* 1934, **38**, **6**, 797-800.
- [13] Monico, L.; Chieli, A.; De Meyer, S.; Cotte, M.; de Nolf, W.; Falkenberg, G.; Janssens, K.; Romani, A.; Miliani, C. Role of the Relative Humidity and the Cd/Zn Stoichiometry in the Photooxidation Process of Cadmium Yellows ($\text{CdS}/\text{Cd}_{1-x}\text{Zn}_x\text{S}$) in Oil Paintings. *Chem. - Eur. J.* **2018**, **24**, 11584-11593.
- [14] Giacometti, L.; Satta, A. Degradation of Cd-yellow paints: Ab initio study of native defects in {10.0} surface CdS. *Microchem. J.* **2016**, **126**, 214-219.
- [15] Giacometti, L.; Satta, A. Reactivity of Cd-yellow pigments: Role of surface defects. *Microchem. J.* **2018**, **137**, 502-508.
- [16] Kresse, G.; Hafner, J. Ab initio molecular dynamics for liquid metals. *Phys. Rev. B* **1993**, **47**, 558-561.
- [17] Kresse, G.; Hafner, J. Ab initio molecular-dynamics simulation of the liquid-metal-amorphous-semiconductor transition in germanium. *Phys. Rev. B* **1994**, **49**, 14251-14269.
- [18] Kresse, G.; Furthmüller, J. Efficiency of ab-initio total energy calculations for metals and semiconductors using a plane-wave basis set. *Comput. Mater. Sci.* **1996**, **6**, 15-10.
- [19] Kresse, G.; Furthmüller, J. Efficient iterative schemes for ab initio total-energy calculations using a plane-wave basis set. *Phys. Rev. B* **1996**, **54**, 11169-11186.
- [20] Perdew, J. P.; Burke, K.; Ernzerhof, M. Generalized Gradient Approximation Made Simple. *Phys. Rev. Lett.* **1996**, **77**, 3865-3868.
- [21] Springer-Verlag Berlin Heidelberg & Material Phases Data System (MPDS), Switzerland & National Institute for Materials Science (NIMS), Japan.
- [22] Partin, D.E.; Okeeffe, M. The structures and crystal chemistry of magnesium chloride and cadmium chloride. *J. Solid State Chem.* **1991**, **95**, 176-183.
- [23] Cudennec, Y.; Riou, A.; Gerault, Y.; Lecerf, A. Synthesis and Crystal Structures of $\text{Cd}(\text{OH})\text{Cl}$ and $\text{Cu}(\text{OH})\text{Cl}$ and Relationship to Brucite Type. *J. Solid State Chem.* **2000**, **151**, 308-312.

- [24] Hinuma, Y.; Gruneis, A.; Kresse, G.; Oba, F. Band alignment of semiconductors from density-functional theory and many-body perturbation theory. *Phys. Rev. B* **2014**, *90*, 155405.
- [25] Banerjee, H.; Barone, P.; Picozzi, S. Half-metallic ferromagnetism in layered CdOHCl induced by hole doping. *2D Mater.* **2021**, *8*, 025027.
- [26] Bader, R. F. W. *Atoms in Molecules: A Quantum Theory*; Clarendon Press: Oxford, 1990.
- [27] Henkelman, G.; Arnaldsson, A.; Jónsson, H. A fast and robust algorithm for Bader decomposition of charge density. *Comput. Mater. Sci.* **2006**, *36*, 354-360.
- [28] Komsa, H.P.; Pasquarello, A. Finite-Size Supercell Correction for Charged Defects at Surfaces and Interfaces. *Phys. Rev. Lett.* **2013**, *110*, 095505.
- [29] Komsa, H.P.; Berseneva, N.; Krasheninnikov, A.V.; Nieminen, R.M. Charged Point Defects in the Flatland: Accurate Formation Energy Calculations in Two-Dimensional Materials. *Phys. Rev. X* **2014**, *4*, 039902.
- [30] Nagakawa, H.; Ochiai, T.; Konuma, S.; Nagata, M. Visible-Light Overall Water Splitting by CdS/WO₃/CdWO₄ Tricomposite Photocatalyst Suppressing Photocorrosion. *ACS Appl. Energy Mater.*, **2018**, *1*, 6730-6735.
- [31] Su, J.; Wei, Y.; Vayssieres, L. Stability and Performance of Sulfide-, Nitride-, and Phosphide-Based Electrodes for Photocatalytic Solar Water Splitting. *J. Phys. Chem. Lett.* **2017**, *8*, 5228–5238.
- [32] Srivastava, O. K.; Secco, E. A. Studies on metal hydroxy compounds. III. Thermal analyses of cadmium derivatives Cd(OH)₂, CdOHCl, and CdOHF. *Can. J. Chem.* **1967**, *45*, 1375-1378.
- [33] Cotte, M.; Pouyet, E.; Salome, M.; Rivard, C.; De Nolf, W.; Castillo-Michel, H.; Fabris, T.; Monico, L.; Janssens, K.; Wang, T. et al. The ID21 X-ray and infrared microscopy beamline at the ESRF: status and recent applications to artistic materials. *J. Anal. At. Spectrom.* **2017**, *32*, 477-493.
- [34] Ravel, B.; Newville, M. ATHENA, ARTEMIS, HEPHAESTUS: data analysis for X-ray absorption spectroscopy using IFEFFIT. *J. Synchrotron Radiat.* **2005**, *12*, 537-541.
- [35] Ganio, M.; Pouyet, E. S.; Webb, S. M.; Patterson, C. M. S; Walton, M.S. From lapis lazuli to ultramarine blue: investigating Cennino Cennini's recipe using sulfur K-edge XANES. *Pure Appl. Chem.* **2018**, *90(3)*, 463-475.

- [36] Monico, L.; Cotte, M.; Vanmeert, F.; Amidani, L.; Janssens, K.; Nuyts, G.; Garrevoet, J.; Falkenberg, G.; Glatzel, P.; Romani, A.; Miliani, C. Damages induced by synchrotron radiation-based X-ray microanalysis in chrome yellow paints and related Cr-compounds: Assessment, quantification, and mitigation strategies. *Anal. Chem.* **2020**, *92*, 14164-14173.
- [37] Bertrand, L.; Schöder, S.; Joosten, I.; Webb, S. M.; Thoury, M.; Calligaro, T.; Anheim, É.; Simon, A. Practical advances towards safer analysis of heritage samples and objects, *TrAC, Trends Anal. Chem.* **2023**, *164*, 117078.
- [38] Godet, M.; Binet, L.; Schoder, S.; Brunel-Duverger, L.; Thoury, M.; Bertrand, L. X-ray irradiation effects on Egyptian blue and green pigments. *J. Anal. At. Spectrom.* **2022**, *37*, 1265-1272.
- [39] Sole, V.A.; Papillon, E.; Cotte, M.; Walter, P.; Susini, J. A multiplatform code for the analysis of energy-dispersive X-ray fluorescence spectra. *Spectrochim. Acta, Part B* **2007**, *62*, 63-68.
- [40] Boesenberg, U.; Ryan, C. G.; Kirkham, R.; Siddons, D. P.; Alfeld, M.; Garrevoet, J.; Nunez, T.; Claussen, T.; Kracht, T.; Falkenberg, G. Fast X-ray microfluorescence imaging with submicrometer-resolution integrating a Maia detector at beamline P06 at PETRA III. *J. Synchrotron Radiat.* **2016**, *23*, 1550-1560
- [41] De Nolf, W.; Vanmeert, F.; Janssens, K. XRDU: Crystalline phase distribution maps by two-dimensional scanning and tomographic (micro) X-ray powder diffraction. *J. Appl. Crystallogr.* **2014**, *47*, 1107-1117.
- [42] Hohenberg, P.; Kohn, W. Inhomogeneous Electron Gas. *Phys. Rev.* **1964**, *136*, B864.
- [43] Kohn, W.; Sham, L. J. Self-Consistent Equations Including Exchange and Correlation Effects. *Phys. Rev.* **1965**, *140*, A1133.
- [44] Blochl, P.E. Projector augmented-wave method. *Phys. Rev. B* **1994**, *50*, 17953-17979.
- [45] Kresse, G.; Joubert, D. From Ultrasoft Pseudopotentials to the Projector Augmented-Wave Method. *Phys. Rev. B* **1999**, *59*, 1758-1775.
- [46] Grimme, S. Semiempirical GGA-type density functional constructed with a long-range dispersion correction. *J. Comput. Chem.* **2006**, *27*, 1787-1799.

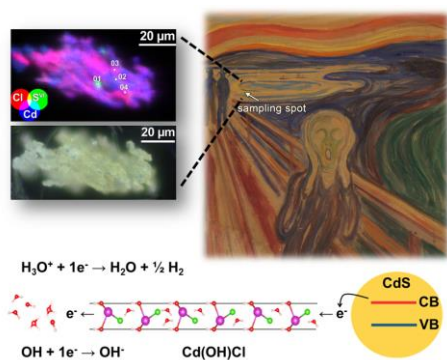
[47] Hinuma, Y.; Gruneis, A.; Kresse, G.; Oba, F. Band alignment of semiconductors from density-functional theory and many-body perturbation theory. *Phys. Rev. B* **2014**, *90*.

[48] Monkhorst, H. J.; Pack, J.D. Special points for Brillouin-zone integrations. *Phys. Rev. B* **1976**, *13*, 5188.

[49] Blöchl, P.E.; Jepsen, O.; Andersen, O.K. Improved tetrahedron method for Brillouin-zone integrations. *Phys. Rev. B* **1994**, *49*, 16223-16233.

Indeed, charged systems that involve a vacuum region cannot be studied when periodic boundary conditions are used within a supercell approach because of the large spurious electrostatic interactions of the charge with its periodic images [28, 29].

Table of content artwork



A Combined Experimental and Computational Approach to Understand CdS Pigment Oxidation in a Renowned Early 20th Century Painting

Selma Mayda^{*[a]}, Letizia Monico^{[b],[c],[d]}, Dileep Krishnan^[a], Steven De Meyer^[d], Marine Cotte^{[e],[f]}, Jan Garrevoet^[g], Gerald Falkenberg^[g], Irina CA Sandu^[h], Bart Partoens^[i], Dirk Lamoen^[a], Aldo Romani^{[b],[c]}, Costanza Miliani^[j], Johan Verbeeck^[a] and Koen Janssens^[d]

[a] Electron Microscopy for Materials Science (EMAT) and NANOLab Center of Excellence, Department of Physics, University of Antwerp, Groenenborgerlaan 171, 2020 Antwerp, Belgium.

[b] CNR-SCITEC, Via Elce di Sotto 8, 06123 Perugia, Italy.

[c] SMAArt Centre of Excellence and Department of Chemistry, Biology, and Biotechnology, University of Perugia via Elce di Sotto 8, 06123 Perugia, Italy.

[d] Antwerp X-ray Imaging and Spectroscopy Laboratory (AXIS) and NANOLab Center of Excellence, Department of Physics, University of Antwerp, Groenenborgerlaan 171, 2020 Antwerp, Belgium.

[e] The European Synchrotron Radiation Facility (ESRF), 38000, Grenoble, France.

[f] Laboratoire d'Archéologie Moléculaire et Structurale (LAMS), Sorbonne Université, CNRS, UMR8220, 4 place Jussieu, 75005 Paris, France.

[g] Deutsches Elektronen-Synchrotron (DESY) Notkestr. 85, 22607 Hamburg, Germany.

[h] MUNCH Museum, Section on Conservation, Edvard Munch plass 1, 0194 Oslo, Norway.

[i] Condensed Matter Theory (CMT) and NANOLab Center of Excellence, Department of Physics, University of Antwerp, Groenenborgerlaan 171, 2020 Antwerp, Belgium.

[j] CNR-ISPC via Cardinale Guglielmo Sanfelice 8, 80134, Naples, Italy.

ABSTRACT: Cadmium sulfide (CdS)-based yellow pigments have been used in a number of early 20th century artworks, including the *Scream* series painted by Edvard Munch. Some of such unique paintings are threatened by the discoloration of CdS-based yellow oil paints because of the oxidation of original sulfides to sulfates. The experimental data prove that moisture and cadmium chlorides play a key role in promoting such oxidation. To clarify how these two factors effectively prompt the process, we studied the band alignment between CdS, CdCl₂, Cd(OH)Cl and the ·OH and H₃O· radicals by density functional theory (DFT) methods. Our results show that a stack of several layers of Cd(OH)Cl creates a pocket of positive holes at the Cl-terminated surface and a pocket of electrons at the OH-terminated surface, by leading in a difference in ionization energy at both surfaces. The resulting band alignment indicates that Cd(OH)Cl can indeed play the role of an oxidative catalyst for CdS in a moist environment, thus providing an explanation to experimental evidence.

Table of Contents

1. Unaged/aged paint mock-ups: STEM-HAADF, STEM-EDX and SR-based X-ray measurements	3
2. Crystal structures of slab CdS, CdCl₂ and Cd(OH)Cl.....	6
3. Charge transfer model for Cd(OH)Cl	7

1. Unaged/aged paint mock-ups: STEM-HAADF, STEM-EDX and SR-based X-ray measurements

Figure S1 illustrates a more detailed view of the intimate mixture of hex-CdS, Cd(OH)Cl and other compounds, such as CdCO₃, that is present in sample 7914_{Cd(OH)Cl} (cf. Figure 3 to see a map recorded from a larger area). Here an irregularly shaped cluster of nanograins is visible, of which it can reasonably be assumed that it mainly consists of CdCO₃, showing the co-presence of high EDX signals of Cd-L, C-K and O-K, but low S-K and Cl-K signals. However, inside this phase, grains are present where no C is present, showing the co-localization of Cd, S and Cl together with weaker O-K signals, consistent with the presence of an intimate hex-CdS/Cd(OH)Cl mixture.

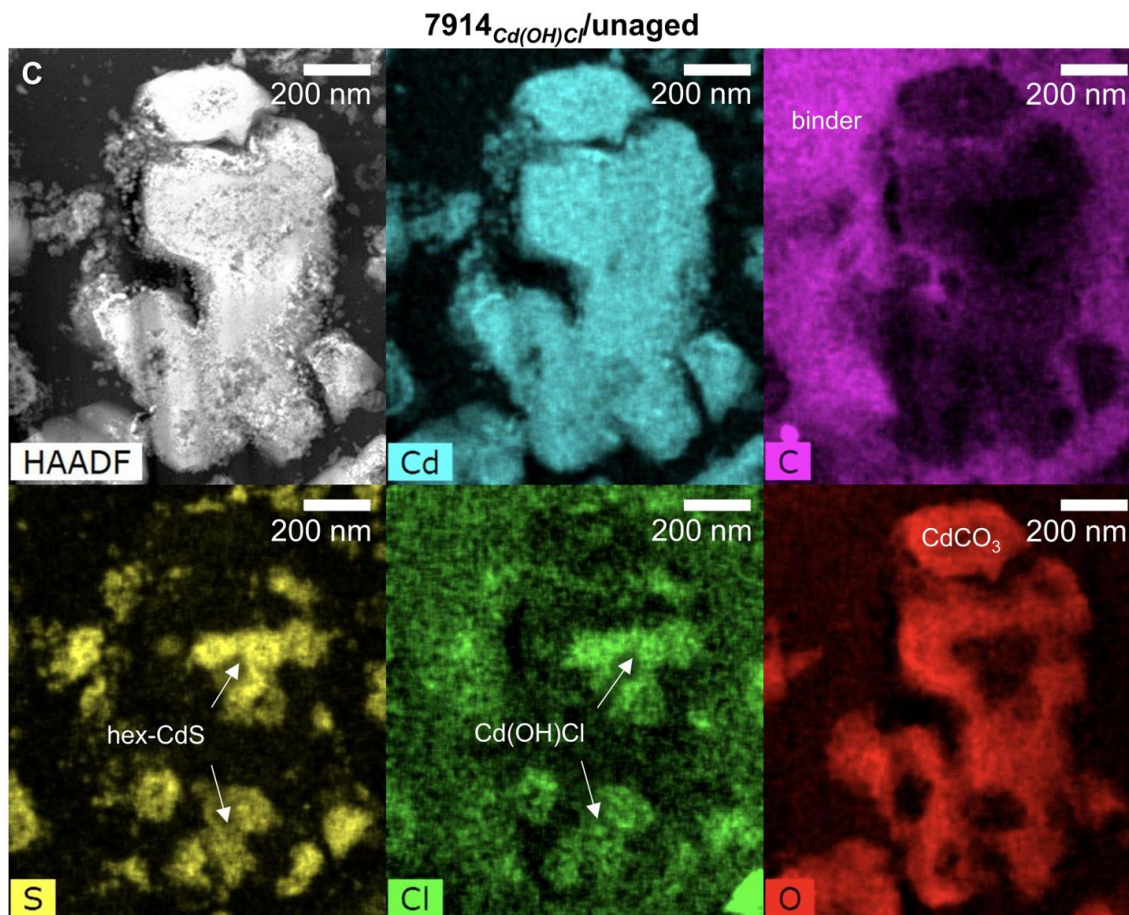


Figure S1. STEM-HAADF image and STEM-EDX maps (Cd-L, C-K, S-K, Cl-K, O-K) of a cluster of nanograins in the unaged historical 7914_{Cd(OH)Cl} paint mock-up showing the intimate mixture of hex-CdS and Cd(OH)Cl on the nanoscale (see Figure 3 to see a map of the entire sample).

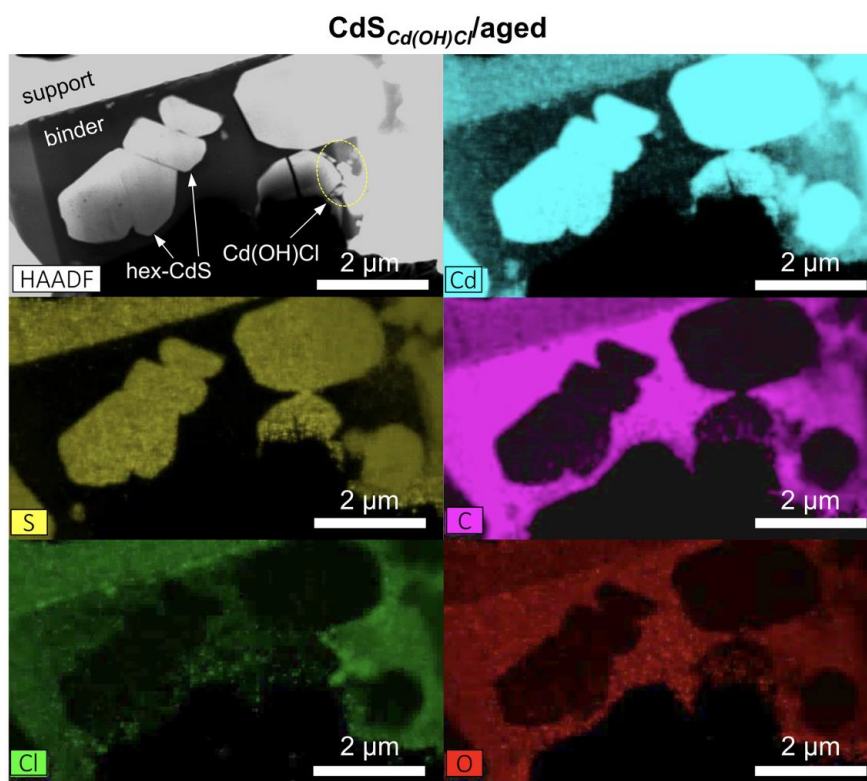


Figure S2. STEM-HAADF image and STEM-EDX maps (Cd-L, S-K, C-K, Cl-K, O-K) of the thermally aged CdS_{Cd(OH)Cl} paint mock-up (RH≥95%, T=40°C, 100 days) prepared as thin section by focused ion beam (FIB) (see Figure 2 for the results from the corresponding unaged paint).

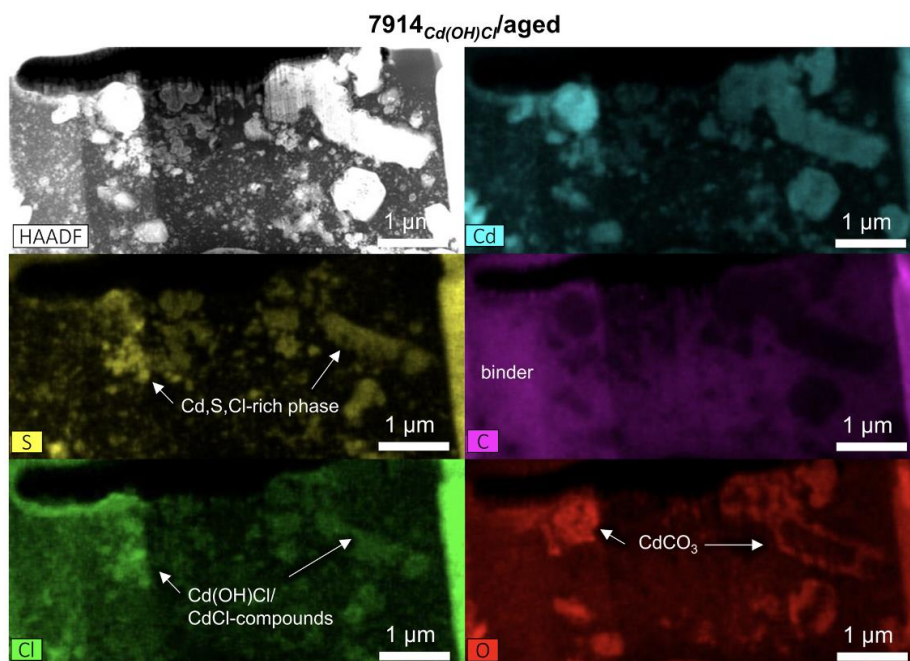


Figure S3. STEM-HAADF image and STEM-EDX maps (Cd-L, S-K, C-K, Cl-K, O-K) of the thermally aged 7914_{Cd(OH)Cl} paint mock-up (RH≥95%, T=40°C, 100 days) prepared as thin section by focused ion beam (FIB) (see Figure 3 for the results from the corresponding unaged paint).

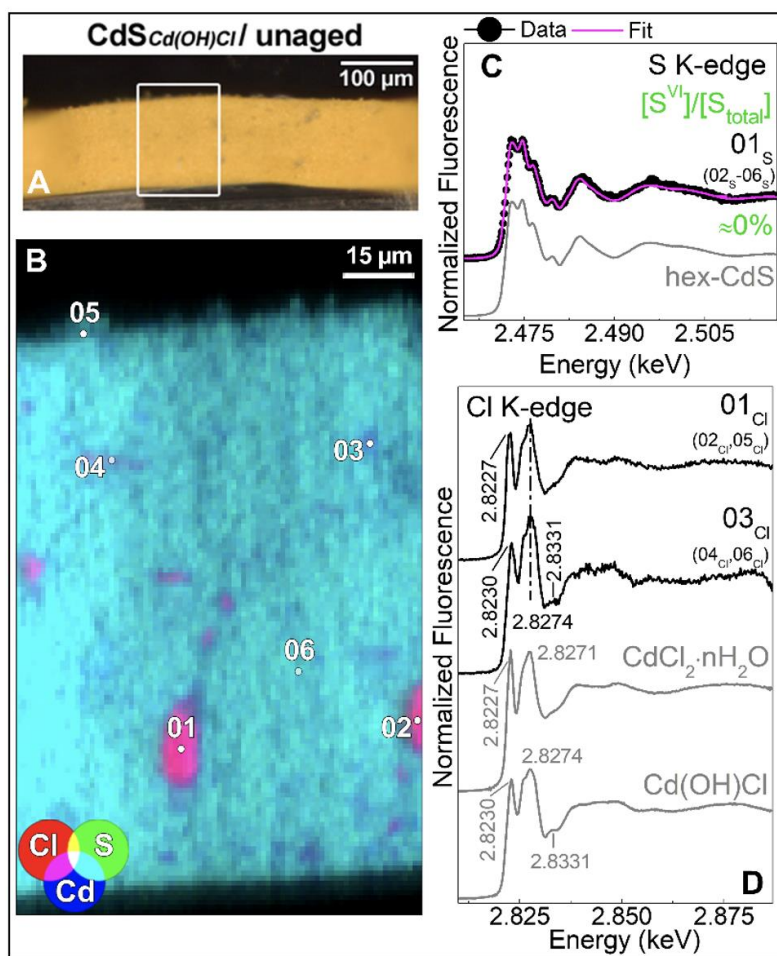


Figure S4. (A) Photomicrograph of unaged $\text{CdS}_{\text{Cd(OH)Cl}}$ thin section and corresponding (B) composite RGB SR μ -XRF images of Cl/S/Cd acquired from the area indicated by the white rectangle in (A) [pixel size ($h \times v$): $2 \times 1 \mu\text{m}^2$, exp. time: 80 ms/pixel]. (C) Selection of (top) S K-edge and (bottom) Cl K-edge μ -XANES spectra (black) collected from the points indicated in (B) and linear combination fitting results (magenta). Numbers in brackets refer to the spectra showing similar features to that reported.

2. Crystal structures of slab CdS, CdCl₂ and Cd(OH)Cl

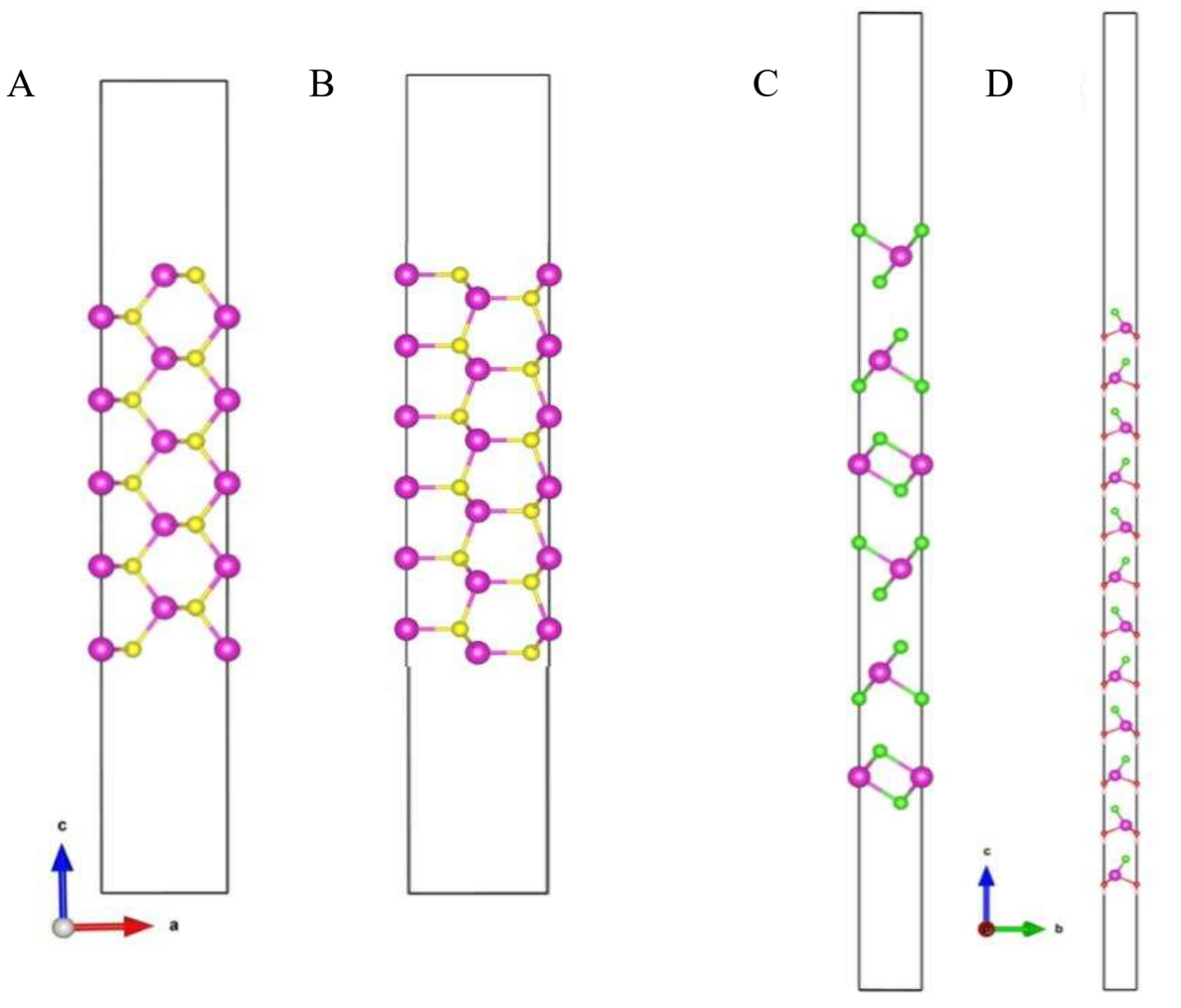


Figure S5. Slab structures of (a) cub-CdS (zincblende structure), (b) hex-CdS (wurtzite structure), (c) CdCl₂ and (d) Cd(OH)Cl. The surface orientation for cub-CdS slabs is (110) and the surface orientation for hex-CdS is (10 $\bar{1}$ 0). For Cd(OH)Cl (in panel (d)), the top surface is Cl-terminated and the bottom surface is OH-terminated (Atom color codes: pink: Cd; yellow: S; green: Cl; red: O; white: H atoms).

3. Charge transfer model for Cd(OH)Cl

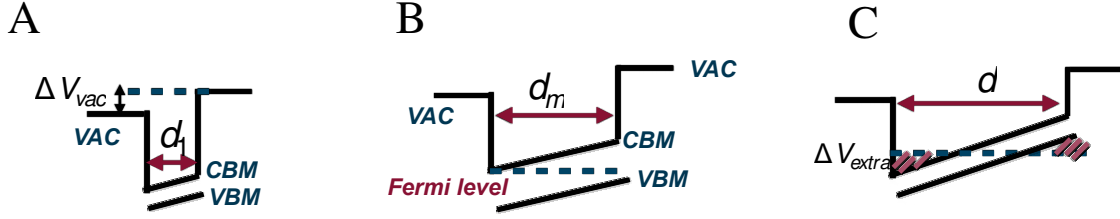


Figure S6. The potential profile for a single layer of Cd(OH)Cl is shown in (A). For a 2-layered Cd(OH)Cl slab, ΔV_{vac} increases as seen in (B) and the total system becomes metallic at a distance d_m . In our model, we show what will happen when more layers are added as in (C) and we want to estimate ΔV_{extra} . Here, the system is modelled as a capacitor.

Figure 7C showed that the difference in vacuum level at both sides of Cd(OH)Cl converges to a fixed value, independent of the number of layers, in spite of the built-in dipole in every single Cd(OH)Cl layer that is added. In this section we propose a simple charge transfer model for Cd(OH)Cl to explain this observation. It therefore also justifies why we can rely on a 12 layer Cd(OH)Cl system to draw conclusions on the band alignment for a general Cd(OH)Cl slab.

A schematic picture of the potential profile over a monolayer of Cd(OH)Cl is illustrated in Figure S6(A). In this Figure d_1 is the thickness of the monolayer Cd(OH)Cl and ΔV_{vac} is the potential difference between the vacuum regions on both sides of the slab. A monolayer of Cd(OH)Cl is a semiconductor and a polar material. If more monolayers are added to the system, ΔV_{vac} will increase and the system will become metallic at a certain distance, say d_m (Figure S6(B)). As shown in Figure S6(C), ΔV_{extra} is now defined as the difference between the Fermi level and the bottom of the conduction band at the OH-terminated Cd(OH)Cl side. A non-zero ΔV_{extra} indicates that the system is metallic. Now we want to understand how ΔV_{extra} evolves when more layers are added and the thickness of the slab d is further increased. Therefore we model the Cd(OH)Cl slab as a capacitor. The work that has to be performed to move a charge Q from the outer Cl-terminated layer to the outer OH-terminated layer is given by

$$W = \int_0^Q \left[-\left(\frac{d-d_m}{d_1}\right) \Delta V_{1layer} + \frac{q}{c} \right] dq = -\frac{d-d_m}{d_1} \Delta V_{1layer} Q + \frac{1}{2} \frac{Q^2}{c} \quad [1]$$

Here ΔV_{1layer} is the built-in potential for a single layer of Cd(OH)Cl. The first term in W gives the energy gain due to the charge transfer over $(d-d_m)/d_1$ layers of Cd(OH)Cl. The second term is the contribution of charging a capacitor. The total charge Q is proportional to ΔV_{extra} (i.e. $Q = \beta \Delta V_{extra}$ for a 2D system) and the capacity is given by $C = \alpha/d$. The total energy of the system now becomes

$$-\frac{d-d_m}{d_1} \beta \Delta V_{1layer} \Delta V_{extra} + \frac{1}{2} \frac{\beta^2 \Delta V_{extra}^2}{\alpha} d \quad [2]$$

Minimizing the energy with respect to ΔV_{extra} gives

$$\frac{\partial W}{\partial \Delta V_{extra}} = -\frac{d-d_m}{d_1} \beta \Delta V_{1layer} + \frac{\beta^2 \Delta V_{extra}}{\alpha} d = 0 \quad [3]$$

from which we can obtain ΔV_{extra} :

$$\Delta V_{extra} = \frac{d-d_m}{d_1} \frac{1}{d} \frac{\alpha}{\beta} \Delta V_{1layer} \quad [4]$$

We find that when d goes to infinity, $d \rightarrow \infty$, ΔV_{extra} becomes independent of the thickness of the system d . This is in agreement with the DFT results presented in Figure 7C of the manuscript: the energy difference between the vacuum levels at both sides of Cd(OH)Cl converges indeed to a fixed value as function of the slab thickness.